Available online at www.sciencedirect.com

ScienceDirect

journal homepage: www.elsevier.com/locate/he

The autothermal reforming of oxymethylenether from the power-to-fuel process

Joachim Pasel[*], *Dirk Schmitt*, *Remzi Can Samsun*, *Andreas Tschauder*, *Ralf Peters*

Forschungszentrum Jülich GmbH, Institute of Energy and Climate Research, IEK-14: Electrochemical Process Engineering, 52425, Jülich, Germany

HIGHLIGHTS

- Use of oxymethylenether (OME_n) as fuel for the autothermal reforming reactions.
- Combining fuel processing for fuel cells with the power-to-fuel process.
- Suitable temperatures in all characteristic sections of reactor ATR 14.
- H_2 concentration in the reformate almost independent of the mass fraction of OME_n.
- Significant reduction in the amount of undesired byproducts (ethene, benzene, etc.)

GRAPHICAL ABSTRACT

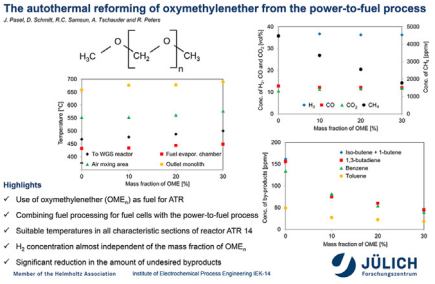

ARTICLE INFO

Article history:
Received 10 May 2021
Received in revised form
28 June 2021
Accepted 30 June 2021
Available online 26 July 2021

Keywords:
Autothermal reforming
Diesel
Power-to-fuel process
Oxymethylenether OME_n
Fuel cell systems
Greenhouse gas emissions

ABSTRACT

Synthetic energy carriers that are not based on crude oil or natural gas can contribute to the transcending of fossil-based sources of energy in the future. A contemporary example is the organic substance, oxymethylenether (OME_n), which consists of hydrogen, carbon, and oxygen. It is reported in the literature that OME_n suppresses the formation of harmful NO_x and soot and reduces CO_2 emissions during the combustion process in internal combustion engines due to its high oxygen content. For the investigation presented in this paper, the use of OME_n was transferred to the autothermal reforming (ATR) process, which is normally conducted using pure diesel fuel or kerosene in order to produce a hydrogen-rich reformate gas to operate fuel cell systems. Different mixtures of OME_n and Ultimate diesel fuel were fed into Jülich's ATR 14 at a steady state. Thereby, approved reaction conditions from former ATR diesel fuel experiments with respect to O_2/C and H_2O/C molar ratios (0.47 and 1.9, respectively) and temperatures of the educts were applied. It was observed that the addition of OME_n to Ultimate diesel fuel resulted in stable temperatures at characteristic positions within ATR 14 and had a positive effect on the quality of the ATR

* *Corresponding author.*
E-mail address: j.pasel@fz-juelich.de (J. Pasel).
https://doi.org/10.1016/j.ijhydene.2021.06.234

product gas (reformate). For instance, the concentration of the undesired byproducts ethene and benzene decreased from 800 ppmv to the range of roughly 230 ppmv and from some 130 ppmv to less than 40 ppmv, respectively, when the mass fraction of OME_n in the OME_n/Ultimate diesel mixture was increased from 0% to 30%.

Introduction

In order to drastically decrease CO_2 emissions in the transport sector and thereby meet the corresponding challenging EU environmental targets, many different technologies are under consideration and technological development. One of these is the so-called power-to-fuel (PtF) process, for which CO_2 separated from the exhaust streams of, e.g., cement or steel facilities and green hydrogen (obtained from water electrolysis [1]) react with each other to generate renewable transport fuels. Among them, oxymethylenether (OME_n) is one possible and promising option. OME_n consists of two terminal methyl groups and different numbers of interjacent formaldehyde units (see Fig. 1), forming a straight-chain molecule whose length depends on the number of inserted formaldehyde units represented by the "n" in the OME_n acronym. Typically, OME molecules feature three, four or five formaldehyde units.

OME_n can be considered a promising alternative to conventional diesel fuels, as in experimental studies it has been found to reduce the emissions of soot, unburnt hydrocarbons, CO, and formaldehyde in internal combustion engines (ICEs) if mixed with conventional diesel fuel or used in pure form [2–13]. Different positions can be found in the literature regarding NO_x emissions when OME_n is used as a fuel in ICEs. Liu et al. [6] observed increasing NO_x emissions with increasing OME_n mass fractions in the fuel. However, there are a considerable number of contributions that report on simultaneous reductions of soot and NO_x emissions when OME_n is used in ICEs [3,11,13]. Additionally, it has been found to be fully soluble in diesel fuel, is non-toxic, and interoperable with the materials used in conventional vehicle ICEs [9]. According to investigations conducted by Lautenschütz et al. [14], Schmitz et al. [15], and Baranowski et al. [16], blends of OME_n molecules with three, four or five formaldehyde units possess physicochemical and combustion characteristics that are comparable to conventional diesel fuel. These include, e.g., density, melting point, flash point, and the auto ignition point, as well as lubricity, kinematic viscosity, and surface tension. Against this background of OME_n being a promising fuel for ICEs, the question arises as to whether it also carries comparable advantages when applied to autothermal reforming (ATR) in the context of fuel cell technology.

With respect to ATR, O_2 (as part of a flow of air) and steam undergo a reaction with a liquid hydrocarbon, such as kerosene, diesel fuel, or their corresponding sulfur and aromatics-free surrogates [17–37] or – as in this study – a mixture of conventional diesel fuel and OME_n. The main products of this reaction are H_2 to be fed into the anode of a fuel cell, CO, CO_2, and CH_4. Undesired side-products in the case of incomplete hydrocarbon conversion could include ethene, ethane, propene, propane, butane, benzene etc. In this respect, Cui and Kaer [38] made thermodynamic analyses to compare different routes to further convert propane and butane: cracking, partial oxidation (POX), steam reforming (SR) and oxidative steam reforming OSR. The authors found olefins and acetylene during cracking and POX and a temperature range between 550 °C and 650 °C, in which the formation of carbon was favored during SR and OSR. Cerqueira et al. [39] investigated ATR and sorption-enhanced ATR of olive mill wastewater by means of a thermodynamic study and energy analysis. They found that the exothermic CO_2 sorption supplies roughly enough energy to make the process thermally neutral. Cherif and Nebbali [40] performed a numerical study about autothermal steam methane reforming. In their concept, CH_4 combustion over a Pt/Al_2O_3 catalyst is responsible for providing heat to the steam reforming of CH_4, which is catalyzed by Ni/Al_2O_3. They investigated three different reactor configurations and found that the third concept for which a copper foam was inserted to increase heat conduction showed the best H_2 yield of 33.48%. In an additional paper, Cherif et al. [41] examined numerically a new reactor design in which the catalysts (Pt/Al_2O_3 for CH_4 combustion and Ni/Al_2O_3 for CH_4 steam reforming) were modeled as patterned thin layers. Here, their results show that if the new concept is used the length of the catalytic zone can be significantly reduced and the consumption of O_2 is diminished by 5%.

ATR is very often a heterogeneously-catalyzed process. In the literature, promising hydrocarbon conversions and technically-meaningful long-term stabilities have been achieved by depositing Ni, Ir, Ru, Pt, and most Rh into porous ceramic supports, such as ZrO_2, SiO_2, perovskites, CeO_2, and Al_2O_3 [42–64]. Han et al. [65–67] followed a somewhat new path for integrating the ATR concept into submarines and replaced O_2 and H_2O by H_2O_2. The latter had to be decomposed in a separate unit prior to being fed into the ATR reactor.

In the literature, there are a few synthesis routes that yield OME_n. As Peters' thermodynamic calculations showed, the direct synthesis of OME_n from CO_2 and H_2 is not favorable from a thermodynamic point of view (i.e., high pressures, low

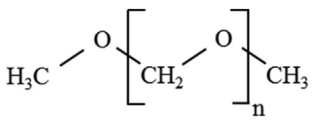

Fig. 1 – Structural formula of OME_n.

temperatures, and side-reactions yielding dimethylether DME) [68], some of the most established pathways to OME_n start from renewable methanol being generated from CO_2 and green H_2 [69].

Pathway a in Fig. 2 entails the direct synthesis of OME_n from 2 mol of methanol and numerous moles of formaldehyde. It is catalyzed by ion-exchange resins [70] and shown in the top panel of Fig. 2 for OME_3. It is advantageous in comparison to the other pathways shown below, as no reaction intermediates are formed [71,72]. However, water being formed in pathway a can lead to undesirable hydrolysis of the OME_n chains, which reduces the yield and selectivity with respect to OME_n [73–75].

Pathway b uses trioxan and OME_1 as educts for the synthesis of OME_n. This is depicted in the middle panel of Fig. 2 for the case of OME_4. Again, the presence of water during this reaction must be avoided in order to ensure that the formed OME_n chains cannot be hydrolyzed. Active catalysts for pathway b are Amberlyst 46 [76], H-ZSM-5 zeolites [77], and molecular sieves [78]. Trioxan is the cyclic trimer of formaldehyde and can be produced from 3 mol of formaldehyde by means of acid catalysts [79]. OME_1, meanwhile, can be formed by a reaction between 2 mol of methanol and 1 mol of formaldehyde [80,81].

Pathway c is the synthesis via dimethylether, as shown in the bottom panel of Fig. 2. One mole of dimethylether reacts with one of trioxan, yielding OME_4 in the case of this particular scheme. Dimethylether can be formed from 2 mol of renewable methanol. A suitable catalyst for pathway c is H-BEA 25, according to a study by Xue et al. [78]. Similar to pathway b, this route also does not yield water, which might hydrolize the OME_n chain again.

The fundamental goal of this study was to compare the operational behavior of Jülich's autothermal reformer generation ATR 14 during steady-state, when it is fed, on the one hand, with conventional Ultimate diesel fuel and, on the other, with blends of Ultimate diesel fuel and OME_n.

Experimental

The constructive improvements in the ATR 14, the way it is operated, and its chemical performance when run with pure Ultimate diesel fuel, are described in detail by Pasel et al. [82]. The design of ATR 14 is shown in Fig. S1 in the Supplementary Material. For that work, a fresh RhPt catalyst on an Al_2O_3–CeO_2 support from Umicore AG & Co. KG was used. For the experiments reported herein, however, a spent RhPt catalyst was utilized that was no longer able to provide hydrocarbon conversions at close to 100% including low molar fractions of unconverted carbon, as previously reported [82]. This approach was selected to highlight the effects of different mass fractions of OME_n in the respective blends with Ultimate diesel fuel on the concentrations of the main products of H_2, CO, CO_2, and CH_4 and undesired byproducts, such as ethene, propene, benzene, etc. Using a fresh catalyst, these possible influences could have been hidden and remained unnoticed due to the catalyst's high initial activity. Ultimate diesel fuel, with a molecular formula of $C_{19}H_{38}$ and molar mass of 266.0 g mol^{-1}, was purchased from ARAL AG. More chemical and technical details with respect to this fuel are provided by Pasel et al. [83]. Table 1 gives an overview of the chemical and physical properties of the OME_n mixture used. It can be seen in this table that it primarily consists of OME_3, OME_4, and OME_5 with a small quantity of OME_6 and only traces of OME_2. This composition results in a molecular formula of $C_{5.66}H_{13.32}O_{4.66}$ and a molar mass of 155.8 g mol^{-1}. For the experiments conducted for this study, this OME_n mixture was in turn blended with Ultimate diesel fuel at different OME_n mass fractions of 10%, 20%, and 30%. For instance, a mixture of 20 ma.% OME and 80 ma.% Ultimate diesel fuel has a molecular formula of $C_{15.01}H_{30.62}O_{1.39}$ and thereby reveals a molar mass of 233.0 g mol^{-1}. Pasel et al. [84] and Meißner et al. [85] describe in detail the analytical apparatus used (FTIR, MS, GC/MS combination) and the methodologies that were employed to quantitatively and qualitatively determine the chemical composition of the dry and gaseous reformate, leaving ATR 14 under the different reaction conditions outlined above. For this study, autothermal reforming was performed with a large excess of water that was condensed downstream of the ATR reactor. The quantities of total organic carbon (TOC) dissolved in the condensed water were analyzed according to the description by Pasel et al. [84].

The following six reactions represent the autothermal reaction network when Ultimate diesel fuel and OME_n are involved. It is interesting to note that the partial oxidation of Ultimate diesel fuel is highly exothermic, whereas that of OME_n is endothermic.

$$C_{19}H_{38} + 9.5\ O_2 \rightarrow 19\ CO + 19H_2\ \Delta H \sim -1790\ kJ\ mol^{-1} \quad (1)$$

$$C_{19}H_{38} + 19H_2O \rightarrow 19\ CO + 38H_2\ \Delta H \sim 2805\ kJ\ mol^{-1} \quad (2)$$

$$C_{5.66}H_{13.32}O_{4.66} + 0.5\ O_2 \rightarrow 5.66\ CO + 6.66H_2\ \Delta H \sim 225\ kJ\ mol^{-1} \quad (3)$$

$$C_{5.66}H_{13.32}O_{4.66} + H_2O \rightarrow 5.66\ CO + 7.66H_2\ \Delta H \sim 346\ kJ\ mol^{-1} \quad (4)$$

$$CO + H_2O \rightarrow CO_2 + H_2\ \Delta H \sim -41\ kJ\ mol^{-1} \quad (5)$$

$$CO + 3H_2 \rightarrow CH_4 + H_2O\ \Delta H \sim -206\ kJ\ mol^{-1} \quad (6)$$

For each experiment reported herein, the O_2/C and H_2O/C molar ratios were kept constant at 0.47 and 1.90, respectively. It is important to note that for calculating the corresponding volumetric flows of air based on the O_2/C molar ratio to run partial oxidation reactions (1) and (3), the additional oxygen atoms from the OME_n chain were not considered. It was assumed that these bonded oxygen atoms would not take part in the partial oxidation reactions, whose kinetics are known to be very fast. 70 vol% of the reaction air was fed into the catalyst via the annular air injector of ATR 14 at a temperature of 380 °C, whereas the residual 30 vol% was injected via the internal superheater at approximately 230 °C, together with 70 ma.% of the water. The residual 30 ma.% of the water was cold and fed into the steam generation chamber of the ATR 14 via a nozzle on the upper side of the autothermal reformer. Another nozzle at the bottom of ATR 14 supplied a spray consisting of small fuel droplets that were injected into

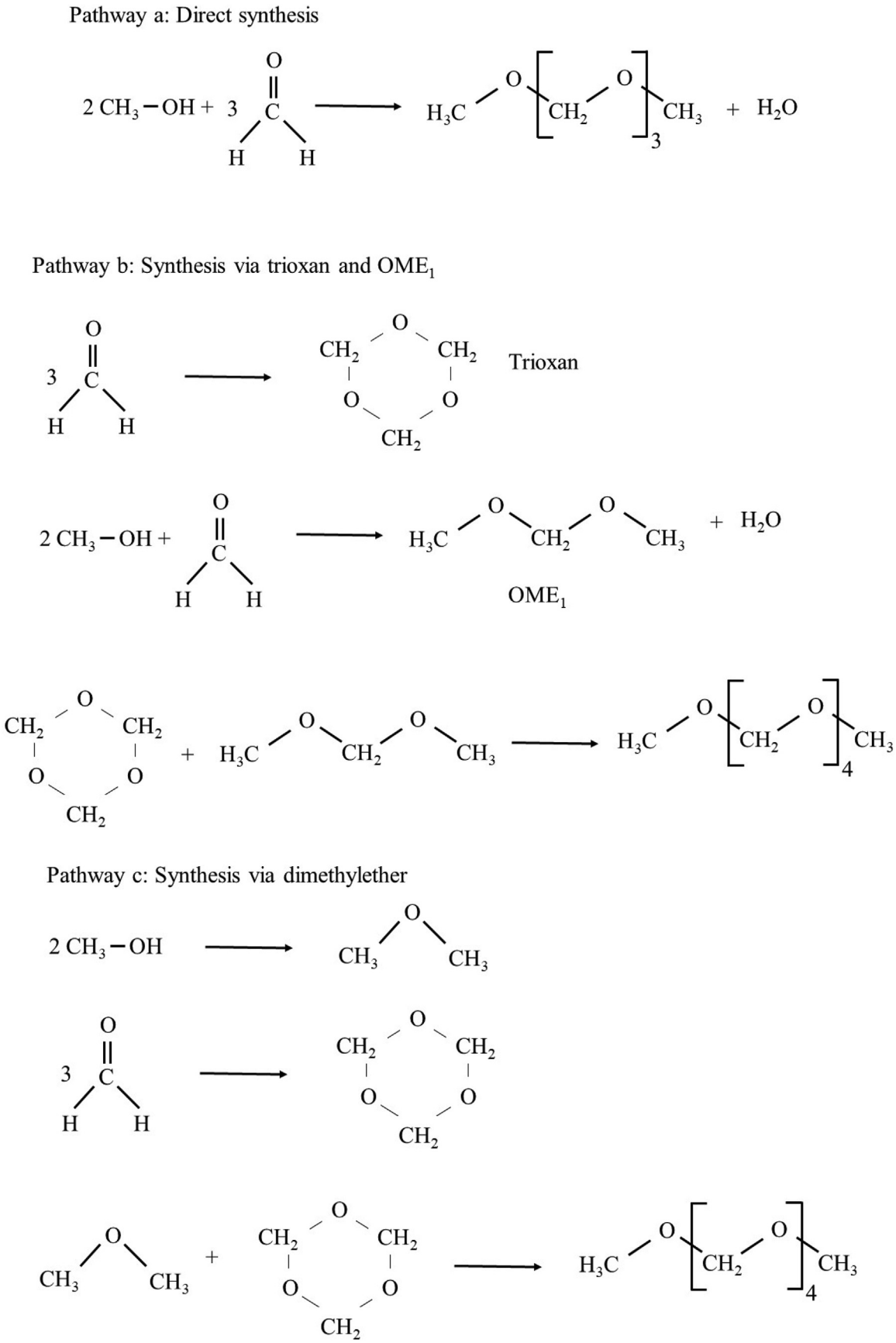

Fig. 2 – Different pathways for the synthesis of oxymethylenether (OME_n) [69]; pathway a: direct synthesis from methanol and formaldehyde; pathway b: synthesis via trioxan and OME_1; pathway c: synthesis via dimethylether.

Table 1 – Chemical and physical properties of the oxymethylenether mixture used during the autothermal reforming experiments.

Parameter	Value	SI-unit
OME_2 content	0.14	ma.%
OME_3 content	46.85	ma.%
OME_4 content	29.23	ma.%
OME_5 content	16.54	ma.%
OME_6 content	5.50	ma.%
Cetane number	73.0	–
Density (15 °C)	1066.1	$kg * m^{-3}$
Sulfur content	<5(<1)	$mg * kg^{-1}$
Flashpoint	66.5	°C
Ash content	<0.001	% (m/m)
Viscosity (40 °C)	1.184	$mm^2 * s^{-1}$
Begin boiling range	152.9	°C
Final boiling point	256.9	°C
Carbon content	43.4	% (m/m)
Hydrogen content	8.6	% (m/m)
Nitrogen content	<0.5	% (m/m)
Oxygen content	45.8	% (m/m)
Lower heating value	19.26	$MJ * kg^{-1}$

the fuel evaporation chamber at room temperature. The reformer's load was varied between 50% and 100%. At 100% load, 2700 g h^{-1} of fuel was fed into the reformer, resulting in a gas hourly space velocity of approximately 26.500 h^{-1} in the catalytically-coated monolith (residence time: approximately 140 ms).

Results and discussion

Fig. 3 presents the temperatures within the ATR 14 when the load was varied between 50% and 100%. In this case, the reformer was operated with a mixture of 80 ma.% Ultimate diesel fuel and 20 ma.% OME_n. The $n(O_2)/n(C)$ and $n(H_2O)/n(C)$ molar ratios were 0.47 and 1.9, respectively, and referred to a molar mass of the fuel blend of 233.0 g mol^{-1}. It can be seen that the temperature at the outlet of the reformer continuously increased, from 678 °C at 50% load to 730 °C at 100% load. In a previous experiment at Jülich with ATR 9.1 [86], an enhancement of the reformer load from 60% to 100% resulted in a significant temperature increase at the outer surface of ATR 9.1 of approximately 30 K, which clearly indicates higher heat losses to the environment at higher loads. However, in order to be able to understand the trend of the temperature at the monolith outlet in Fig. 3, the values of the reaction enthalpy of the partial oxidation in equation (1) must also be considered. It is only half the quantity at 50% load compared to 100%. As the thermodynamic calculations showed that the absolute values of the reaction enthalpy of the partial oxidation were much higher than those of the corresponding heat losses to the environment, it becomes clear that the temperature at the outlet of the monolith has to rise with the increasing reformer load. For the same reason, the temperature of the reformate flowing to the downstream water-gas shift reactor (if a system configuration is taken into consideration) increased from 482 °C at 50% load to 517 °C at 100% load. At the same time, the temperatures in the air mixing

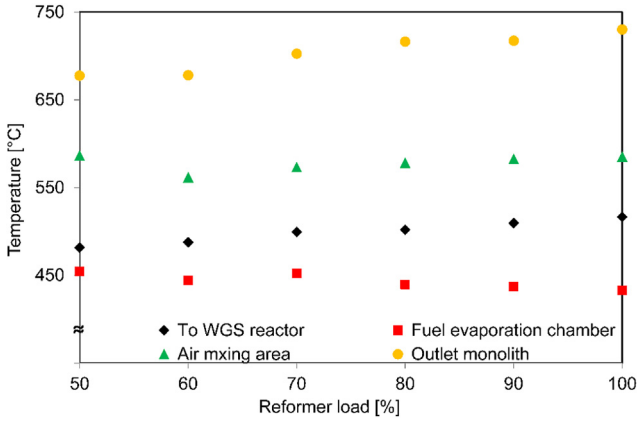

Fig. 3 – Temperatures inside ATR 14 when the load of the ATR was varied between 50% and 100%. The ATR was operated with a mixture of 80 ma.% Ultimate diesel fuel and 20 ma.% OME_n, $n(O_2)/n(C) = 0.47$, and $n(H_2O)/n(C) = 1.9$, with the mass fraction of cold water to the nozzle being 30%.

area were fairly stable between 586 °C at partial load and 585 °C at full load, and only slightly varied between 454 °C and 432 °C in the fuel evaporation chamber. In both areas, the temperatures were high enough to guarantee that all molecules of Ultimate diesel fuel and OME_n were fully vaporized prior to entering the monolith and coming into contact with the catalyst. The comparably high temperature levels in the air mixing area and fuel evaporation chamber were due to the non-catalytic homogeneous gas phase reaction between O_2 and lighter hydrocarbon molecules in diesel fuel and OME_n. From Fig. 3, it can be concluded that ATR 14 can be smoothly operated with a mixture of 80 ma.% Ultimate diesel and 20 ma.% OME_n under the given reaction conditions if the temperatures are taken into account. The next two figures shed some light on the corresponding gas concentrations in the dry reformate of ATR 14.

Fig. 4 depicts the concentrations of H_2, CO, CO_2, and CH_4 in the dry reformate of ATR 14 under the same reaction conditions as applied in the experiments in Fig. 3. The H_2 concentrations exhibited a decreasing trend from 36.3 vol% to 34.8 vol % when the load was increased. The same trend holds true for the CO_2 concentration, with a decrease from 11.5 vol% at 50% load to 10.2 vol%, while in parallel the concentration of CO rose from 12.1 vol% to 13.5 vol%. On the one hand, these three concentration trends can be explained by a shift in the thermodynamic equilibrium of the exothermic water-gas shift reaction (equation (5)) to the educt side as the temperature at the outlet of the monolith increased (cf. Fig. 3). On the other hand, during autothermal reforming, increasing CO and decreasing H_2 concentrations always indicate enhancing side reactions, which in turn produce undesired byproducts, such as ethene, propene or benzene, etc. [84]. In the case of the CH_4 concentration, a significant increase, from approximately 2220 ppmv at 50% load to more than 4000 ppmv at 100% load, was observed. This trend, however, cannot be explained by thermodynamics, as the CH_4 concentration should have decreased with rising temperature, as per the methanation reaction cited in equation (6). In this case, it can be concluded

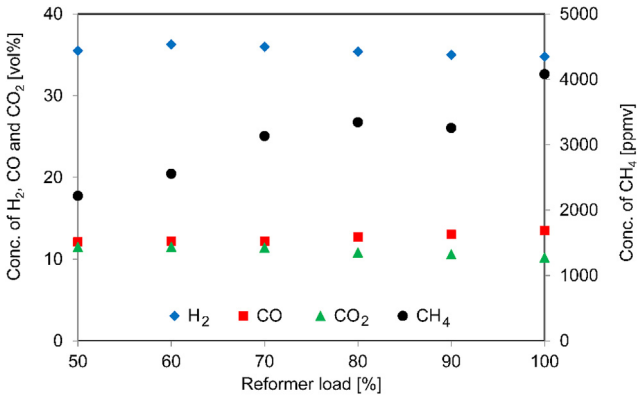

Fig. 4 – Concentrations of H_2, CO, CO_2, and CH_4 in the dry reformate when the load of the ATR was varied between 50% and 100%. The ATR was operated with a mixture of 80 ma.% Ultimate diesel fuel and 20 ma.% OME_n, $n(O_2)/n(C) = 0.47$ and $n(H_2O)/n(C) = 1.9$, with the mass fraction of cold water to the nozzle being 30%.

that decreasing the hydrodynamic residence times of the reaction mixture on the catalyst surface favored the methanation reaction to the detriment of the reactions, as per equations (1)–(4).

In this respect, Fig. 5 provides additional information regarding the relevance of undesired side reactions. It shows the concentrations of ethene, propene, and benzene in the dry reformate, again under the same reaction conditions as applied in the experiments in Fig. 3. The concentration of benzene was almost constant throughout the entire load range, and those of ethene and propene had increasing trends from 210 ppmv to 380 ppmv and 140 ppmv to 190 ppmv, respectively. This figure strengthens the finding displayed from Fig. 4 that side reactions are favored by shorter reactant residence times on the catalyst surface. Although the RhPt catalyst was already spent at the beginning of the experiments conducted for this study, the last two figures pertaining to the concentrations in the reformate allow the conclusion to be drawn that adding OME_n to Ultimate diesel fuel is not detrimental to the autothermal reforming network. For the following figures, different mass fractions of OME_n in the OME_n/Ultimate diesel mixtures were applied to learn more about the influence of OME_n on the relevant parameters of autothermal reforming.

Fig. 6 illustrates the temperatures within the ATR 14 when the mass fraction of OME_n in the Ultimate/OME_n mixture was varied between 0% and 30% at a reformer load of 60%. The $n(O_2)/n(C)$ and $n(H_2O)/n(C)$ molar ratios were still 0.47 and 1.9, respectively. It becomes clear that all four characteristic temperatures inside the ATR 14 featured a slightly increasing trend when the mass fraction of OME_n in the OME_n/Ultimate diesel mixture grew from 0% to 30%. E.g., those in the fuel evaporation chamber rose from 432 °C to 449 °C, whereas those of the reformate at the outlet of the monolith increased from 659 °C to 690 °C. One possible explanation can be found in the different boiling ranges of Ultimate diesel fuel and OME_n. The final boiling point of Ultimate diesel is approximately 360 °C [83], whereas that of OME_n is about 257 °C (see Table 1). It can be concluded from this significant difference that the quantity of lighter hydrocarbons is higher in OME_n than it is in Ultimate diesel fuel and, therefore, is further enhanced in the OME_n/Ultimate diesel mixture with increasing mass fractions of OME_n. Lighter hydrocarbons were found to more easily react in the above-mentioned homogeneous pre-reaction in the evaporation chamber and air-mixing area. This in turn led to higher temperatures in these sections of the ATR 14, when the OME_n mass fraction rose. Additionally, it is conceivable that O-atoms or O-containing fragments being released from reacting and decomposing OME_n molecules favored the exothermic partial oxidation of the present hydrocarbon molecules, which resulted in

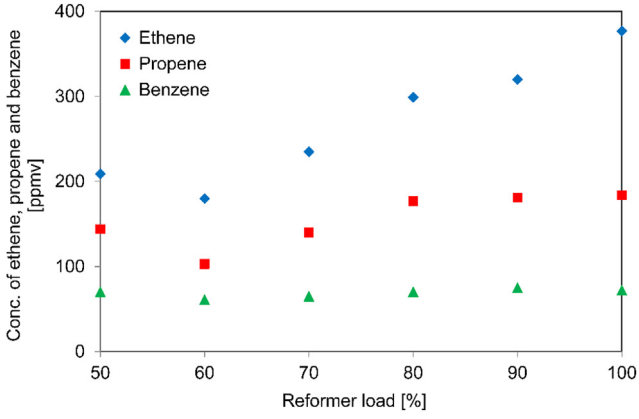

Fig. 5 – Concentrations of ethene, propene, and benzene in the dry reformate when the load of the ATR was varied between 50% and 100%. The ATR was operated with a mixture of 80 ma.% Ultimate diesel fuel and 20 ma.% OME_n, $n(O_2)/n(C) = 0.47$, $n(H_2O)/n(C) = 1.9$, with a mass fraction of cold water to the nozzle of 30%.

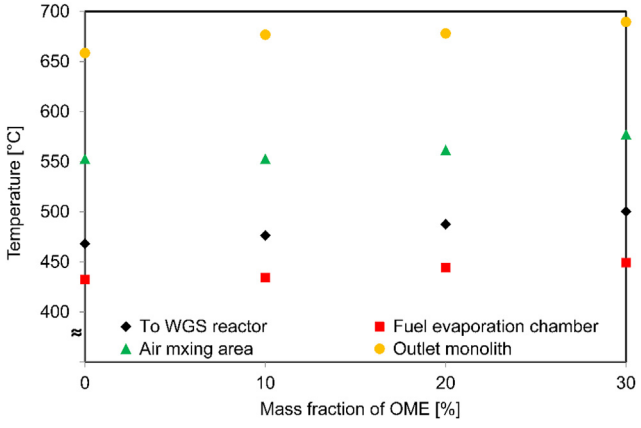

Fig. 6 – Temperatures inside the ATR 14 when the mass fraction of OME_n in the Ultimate/OME_n mixture was varied between 0% and 30% at a reformer load of 60%, $n(O_2)/n(C) = 0.47$, $n(H_2O)/n(C) = 1.9$, and the mass fraction of cold water to the nozzle was 30%.

enhancing the temperatures of the reformate at the outlet of the monolith and at the position where it was fed to the downstream WGS-reactor. Of course, the higher the mass fraction of OME_n in the OME_n/Ultimate diesel mixture, the stronger this effect was.

Fig. 7 depicts the concentrations of H_2, CO, CO_2, and CH_4 in the dry reformate of ATR 14 when the mass fraction of OME_n in the Ultimate/OME_n mixture was varied between 0% and 30% at a reformer load of 60% ($n(O_2)/n(C) = 0.47$ and $n(H_2O)/n(C) = 1.9$). Although the concentrations of H_2 varied slightly between 36.3 vol% and 36.7 vol%, those of CO and CO_2 showed decreasing (from 12.8 vol% to 12.0 vol%) and increasing (from 10.5 vol% to 11.8 vol%) trends, respectively. A strong decrease in the concentrations in the reformate from approximately 4500 ppmv, when only Ultimate diesel fuel was utilized, to less than 2000 ppmv at an OME_n mass fraction of 30% was observed in the case of CH_4. Thus, increasing the mass fraction of OME_n in the OME_n/Ultimate diesel mixture was found to be highly beneficial for the concentrations of the main products of autothermal reforming and, consequently, for the operation of ATR 14. Once again, the more favorable boiling range of OME_n by comparison to Ultimate diesel fuel could have been the reason for this advantage. Lighter hydrocarbons more easily fully evaporate and homogeneously mix with the other reactants, O_2 and H_2O. In order to evaluate this finding, the last figure presented below deals with the corresponding trends of some undesired gaseous by-products in the dry reformate and the quantity of total organic carbon (TOC) dissolved in the unconverted stream of water, which was condensed downstream the ATR 14.

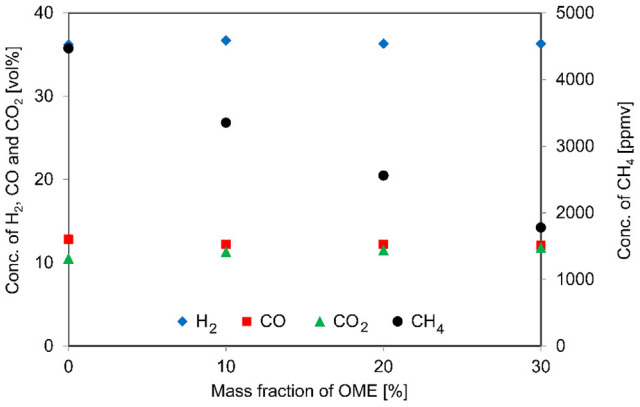

Fig. 7 – Concentrations of H_2, CO, CO_2, and CH_4 in the dry reformate of ATR 14 when the mass fraction of OME_n in the Ultimate/OME_n mixture was varied between 0% and 30% at a reformer load of 60%, $n(O_2)/n(C) = 0.47$, $n(H_2O)/n(C) = 1.9$, and the mass fraction of cold water to the nozzle was 30%.

Fig. 8(a–c) illustrate the concentrations of different undesired byproducts of autothermal reforming in the dry gas phase at the outlet of the ATR 14, when the mass fraction of OME_n in the OME_n/Ultimate diesel mixture increased from 0% to 30%. The molar educt ratios again remained the same. The values of each byproduct exhibit the same decreasing trends, however, at different concentration levels. In Fig. 8 (a), for instance, the concentration of ethene decreased from approximately 800 ppmv to the range of roughly 230 ppmv, whereas in Fig. 8 (b), the values for 1,3-butadiene diminished from more than 150 ppmv to approximately 50 ppmv. Another example is the concentration of 1-pentene in Fig. 8 (c), which fell from some 30 ppmv to less than 10 ppmv. Additionally, Fig. 8 (d) displays the quantities of total organic carbon (TOC) in the unconverted, condensed water downstream the ATR 14

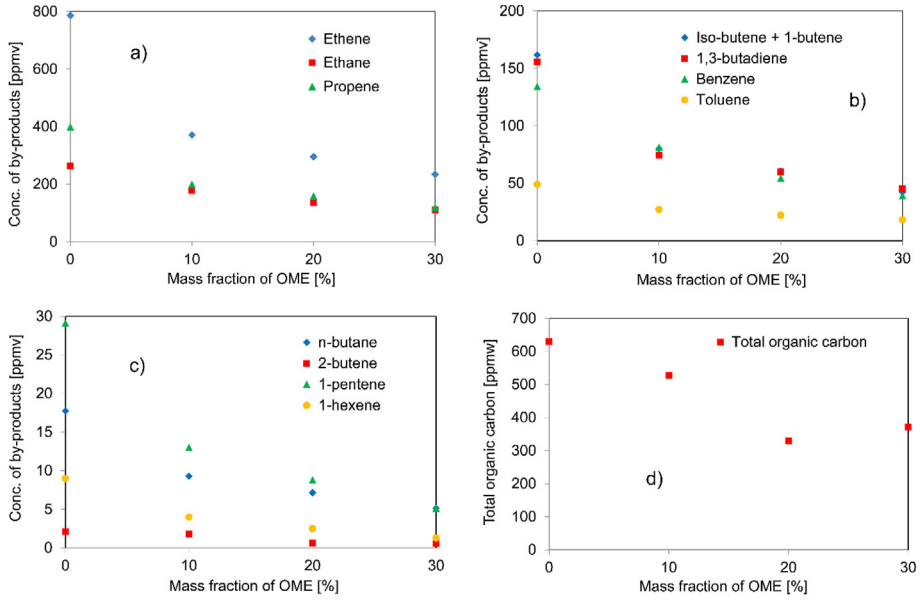

Fig. 8 – Concentrations of byproducts in the dry reformate of the ATR 14 (a)–(c) and the quantities of total organic carbon in the unconverted, condensed water downstream ATR 14 (d), when the mass fraction of OME_n in the Ultimate/OME_n mixture was varied between 0% and 30% at a reformer load of 60%, $n(O_2)/n(C) = 0.47$, $n(H_2O)/n(C) = 1.9$, and the mass fraction of cold water to the nozzle was 30%.

under the same reaction conditions. They show the same decreasing trend with an increasing mass fraction of OME_n from more than 600 ppmw to approximately 350 ppmw. These four figures stress the above-given finding that increasing the mass fraction of OME_n in the educt mixture has a plainly positive effect on the operational behavior of the ATR 14.

Conclusions

Many studies can be found in the literature that deal with the autothermal reforming of diesel and jet fuel. These fuels differ from one another in terms of their original feedstock (i.e., crude oil, synthesis gas, renewable primary products, etc.), sulfur contents, mass fractions of aromatics, boiling ranges, etc. This study expands the spectrum of fuels for experimental evaluation for autothermal reforming through a fuel obtained from the Power-to-Fuel process: oxymethylenether (OME_n). In the experiments, OME_n was blended with conventional Ultimate diesel fuel at mass fractions of between 0% and 30% and, additionally, the load of the autothermal reformer was varied between 50% and 100%. It was found that adding OME_n to Ultimate diesel fuel positively affected the operation of the ATR 14 autothermal reformer with respect to the temperatures in all characteristic sections of the unit, the concentrations of the main products of the process (i.e., H_2, CO, CO_2, and CH_4), and most of all if the concentrations of undesired byproducts are taken into account. The quantities in the reformate of the ATR 14 were by far lowest, at the highest mass fraction of OME_n of 30% applied in this work. The significantly higher quantity of lighter hydrocarbons in OME_n might have favored the homogeneous pre-reaction in the fuel evaporation chamber and the air mixing area of ATR 14. This resulted in higher temperatures in these reactor sections, when the mass fraction of OME_n in the OME_n/Ultimate diesel mixture increased. Additionally, an enhancing quantity of O-atoms and O-containing fragments from reacting and decomposing OME_n molecules might have favored the partial oxidation of the available hydrocarbon molecules. This in turn increased the temperatures in the catalyst. Both effects of increased OME_n mass fractions – favored homogeneous pre-reaction and more intense partial oxidation – raised the overall temperature level in all sections of ATR 14, fostered the catalytic conversion and, thereby, decreased the quantities of byproducts, such as ethene, benzene or 1,3-butadiene. This beneficial influence of OME_n is somewhat comparable to the consistently positive results that have been reported in the literature in relation to the emissions of soot, unburnt hydrocarbons, CO, and NO_x, when OME_n was used in ICEs. The results of this paper allow for the general conclusion to be drawn that the use of OME_n as an additive fuel for the autothermal reforming network is beneficial to the process.

Declaration of competing interest

The authors declare that they have no known competing financial interests or personal relationships that could have appeared to influence the work reported in this paper.

Acknowledgements

Special thanks are due to the fuel processing team at Jülich and all project and cooperation partners.

Appendix A. Supplementary data

Supplementary data to this article can be found online at https://doi.org/10.1016/j.ijhydene.2021.06.234.

REFERENCES

[1] Li N, Araya SS, Cui X, Kær SK. The effects of cationic impurities on the performance of proton exchange membrane water electrolyzer. J Power Sources 2020;473:228617. https://doi.org/10.1016/j.jpowsour.2020.228617.
[2] Gaukel K, Pélerin D, Härtl M, Wachtmeister G, Burger J, Maus W, et al. The fuel OME2: an example to pave the way to emission-neutral vehicles with internal combustion engine. In: Lenz H-P, editor. 37th international vienna motor symposium, fortschrittsberichte VDI series 12. Düsseldorf: VDI-Verlag; 2016. p. 193–223.
[3] Härtl M, Gaukel K, Pélerin D, Wachtmeister G. Oxymethylenether als potenziell CO2-neutraler Kraftstoff für saubere Dieselmotoren, Teil 1: Motorenuntersuchungen. Motortechnische Zeitschrift 2017;78:52–9.
[4] Iannuzzi SE, Barro C, Boulouchos K, Burger J. Combustion behavior and soot formation/oxidation of oxygenated fuels in a cylindrical constant volume chamber. Fuel 2016;167:49–59.
[5] Liu H, Wang Z, Wang J, He X. Improvement of emission characteristics and thermal efficiency in diesel engines by fueling gasoline/diesel/PODEn blends. Energy 2016;97:105–12. https://doi.org/10.1016/j.energy.2015.12.110.
[6] Liu H, Wang Z, Zhang J, Wang J, Shuai S. Study on combustion and emission characteristics of Polyoxymethylene Dimethyl Ethers/diesel blends in light-duty and heavy-duty diesel engines. Appl Energy 2017;185:1393–402. https://doi.org/10.1016/j.apenergy.2015.10.183.
[7] Liu H-y, Wang Z, Wang J-X. Performance, combustion and emission characteristics of polyoxymethylene dimethyl ethers ($PODE_{3-4}$)/Wide distillation fuel (WDF) blends in premixed low temperature combustion (LTC). SAE Int J Fuels Lubricants 2015;8:298–306.
[8] Liu J, Wang H, Li Y, Zheng Z, Xue Z, Shang H, et al. Effects of diesel/PODE (polyoxymethylene dimethyl ethers) blends on combustion and emission characteristics in a heavy duty diesel engine. Fuel 2016;177:206–16. https://doi.org/10.1016/j.fuel.2016.03.019.
[9] Lumpp B, Rothe D, Pastötter C, Lämmermann R, Jacob E. Oxymethylene ethers as diesel fuel additives OF the future. MTZ worldwide eMagazine 2011;72:34–8. https://doi.org/10.1365/s38313-011-0027-z.
[10] Pellegrini L, Marchionna M, Patrini R, Beatrice C, Del Giacomo N, Guido C. Combustion behavior and emission performance of neat and blended polyoxymethylene dimethyl ethers in a light-duty engine. Detroit, USA: SAE 2012 World Congress & Exhibition; 2012.
[11] Ren Y, Huang Z, Miao H, Di Y, Jiang D, Zeng K, et al. Combustion and emissions of a DI diesel engine fuelled with

diesel-oxygenate blends. Fuel 2008;87:2691–7. https://doi.org/10.1016/j.fuel.2008.02.017.
[12] Wang Z, Liu H, Zhang J, Wang J, Shuai S. Performance, combustion and emission characteristics of a diesel engine fueled with polyoxymethylene dimethyl ethers (PODE3-4)/Diesel blends. Energy Procedia 2015;75:2337–44. https://doi.org/10.1016/j.egypro.2015.07.479.
[13] Yuvarajan D, Ravikumar J, Babu MD. Simultaneous optimization of smoke and NOx emissions in a stationary diesel engine fuelled with diesel–oxygenate blends using the grey relational analysis in the Taguchi method. Analytical Methods 2016;8:6222–30. https://doi.org/10.1039/C6AY01696K.
[14] Lautenschütz L, Oestreich D, Seidenspinner P, Arnold U, Dinjus E, Sauer J. Physico-chemical properties and fuel characteristics of oxymethylene dialkyl ethers. Fuel 2016;173:129–37. https://doi.org/10.1016/j.fuel.2016.01.060.
[15] Schmitz N, Burger J, Ströfer E, Hasse H. From methanol to the oxygenated diesel fuel poly(oxymethylene) dimethyl ether: an assessment of the production costs. Fuel 2016;185:67–72. https://doi.org/10.1016/j.fuel.2016.07.085.
[16] Baranowski CJ, Bahmanpour AM, Kröcher O. Catalytic synthesis of polyoxymethylene dimethyl ethers (OME): a review. Appl Catal, B 2017;217:407–20. https://doi.org/10.1016/j.apcatb.2017.06.007.
[17] Dong J, Xu XH, Xu B, Zhang SY. Parametric analysis of a solid oxide fuel cell auxiliary power unit operating on syngas produced by autothermal reforming of hydrocarbon fuels. J Renew Sustain Energy 2016;8. https://doi.org/10.1063/1.4945572.
[18] García-Díez E, García-Labiano F, de Diego LF, Abad A, Gayán P, Adánez J. Autothermal chemical looping reforming process of different fossil liquid fuels. Int J Hydrogen Energy 2017;42:13633–40. https://doi.org/10.1016/j.ijhydene.2016.12.109.
[19] González AV, Pettersson LJ. Full-scale autothermal reforming for transport applications: the effect of diesel fuel quality. Catal Today 2013;210:19–25. https://doi.org/10.1016/j.cattod.2012.11.009.
[20] Harada M, Takanabe K, Kubota J, Domen K, Goto T, Akiyama K, et al. Hydrogen production by autothermal reforming of kerosene over MgAlOx-supported Rh catalysts. Appl Catal, A 2009;371:173–8. https://doi.org/10.1016/j.apcata.2009.10.009.
[21] Jeong S, Kim D, Lee JH. Modeling and simulation of autothermal reforming reactor of diesel over Ni-based catalyst in solid oxide fuel cell based auxiliary power unit system. Computer Aided Chemical Engineering; 2018. p. 613–8.
[22] Kaila RK, Gutiérrez A, Krause AOI. Autothermal reforming of simulated and commercial diesel: the performance of zirconia-supported RhPt catalyst in the presence of sulfur. Appl Catal, B 2008;84:324–31. https://doi.org/10.1016/j.apcatb.2008.04.007.
[23] Kaila RK, Krause AOI. Autothermal reforming of simulated gasoline and diesel fuels. Int J Hydrogen Energy 2006;31:1934–41. https://doi.org/10.1016/j.ijhydene.2006.04.004.
[24] Kang I, Bae J. Autothermal reforming study of diesel for fuel cell application. J Power Sources 2006;159:1283–90. https://doi.org/10.1016/j.jpowsour.2005.12.048.
[25] Kang I, Bae J, Bae G. Performance comparison of autothermal reforming for liquid hydrocarbons, gasoline and diesel for fuel cell applications. J Power Sources 2006;163:538–46. https://doi.org/10.1016/j.jpowsour.2006.09.035.
[26] Karatzas X, Creaser D, Grant A, Dawody J, Pettersson LJ. Hydrogen generation from n-tetradecane, low-sulfur and Fischer–Tropsch diesel over Rh supported on alumina doped with ceria/lanthana. Catal Today 2011;164:190–7. https://doi.org/10.1016/j.cattod.2010.10.019.
[27] Lin L, Wu LQ, Sui LR, He SH. Autothermal reforming of diesel to hydrogen and activity evaluation. Energy Fuel 2018;32:7971–7. https://doi.org/10.1021/acs.energyfuels.8b01431.
[28] Liu D-J, Kaun TD, Liao H-K, Ahmed S. Characterization of kilowatt-scale autothermal reformer for production of hydrogen from heavy hydrocarbons. Int J Hydrogen Energy 2004;29:1035–46. https://doi.org/10.1016/j.ijhydene.2003.11.009.
[29] Shi L, Bayless DJ, Prudich ME. A CFD model of autothermal reforming. Int J Hydrogen Energy 2009;34:7666–75. https://doi.org/10.1016/j.ijhydene.2009.07.039.
[30] Walluk MR, Lin J, Waller MG, Smith DF, Trabold TA. Diesel auto-thermal reforming for solid oxide fuel cell systems: anode off-gas recycle simulation. Appl Energy 2014;130:94–102. https://doi.org/10.1016/j.apenergy.2014.04.064.
[31] Xu X, Zhang S, Li P. Autothermal reforming of n-dodecane and desulfurized Jet-A fuel for producing hydrogen-rich syngas. Int J Hydrogen Energy 2014;39:19593–602. https://doi.org/10.1016/j.ijhydene.2014.09.124.
[32] Xu X, Zhang S, Wang X, Li P. Fuel adaptability study of a lab-scale 2.5 kWth autothermal reformer. Int J Hydrogen Energy 2015;40:6798–808. https://doi.org/10.1016/j.ijhydene.2015.03.147.
[33] Zhang S, Wang X, Xu X, Li P. Hydrogen production via catalytic autothermal reforming of desulfurized Jet-A fuel. Int J Hydrogen Energy 2017;42:1932–41. https://doi.org/10.1016/j.ijhydene.2016.11.004.
[34] Danilov VA, Kolb G. Tanks-in-series model for an auto-thermal reforming reactor with a channeled monolith. Chem Eng Sci 2021:231. https://doi.org/10.1016/j.ces.2020.116269.
[35] Malik FR, Tieqing Z, Kim YB. Temperature and hydrogen flow rate controls of diesel autothermal reformer for 3.6 kW PEM fuel cell system with autoignition delay time analysis. Int J Hydrogen Energy 2020;45:29345–55. https://doi.org/10.1016/j.ijhydene.2020.07.208.
[36] Song Y, Han K, Wang DY. Thermodynamic analysis of fossil fuels reforming for fuel cell application. Int J Hydrogen Energy 2020;45:20232–9. https://doi.org/10.1016/j.ijhydene.2019.11.175.
[37] Zazhigalov SV, Rogozhnikov VN, Snytnikov PV, Potemkin DI, Simonov PA, Shilov VA, et al. Simulation of diesel autothermal reforming over Rh/Ce0.75Zr0.25O2-δ-η-Al2O3/FeCrAl wire mesh honeycomb catalytic module. Chemical Engineering and Processing - Process Intensification 2020:150. https://doi.org/10.1016/j.cep.2020.107876.
[38] Cui X, Kær SK. Thermodynamic analysis of steam reforming and oxidative steam reforming of propane and butane for hydrogen production. Int J Hydrogen Energy 2018;43:13009–21. https://doi.org/10.1016/j.ijhydene.2018.05.083.
[39] Cerqueira P, Soria MA, Madeira LM. Combined autothermal and sorption-enhanced reforming of olive mill wastewater for the production of hydrogen: thermally neutral conditions analysis. Int J Hydrogen Energy 2021. https://doi.org/10.1016/j.ijhydene.2021.04.189.
[40] Cherif A, Nebbali R. Numerical analysis on autothermal steam methane reforming: effects of catalysts arrangement and metal foam insertion. Int J Hydrogen Energy 2019;44:22455–66. https://doi.org/10.1016/j.ijhydene.2018.12.203.
[41] Cherif A, Nebbali R, Sheffield JW, Doner N, Sen F. Numerical investigation of hydrogen production via autothermal reforming of steam and methane over Ni/Al2O3 and Pt/Al2O3

patterned catalytic layers. Int J Hydrogen Energy 2021. https://doi.org/10.1016/j.ijhydene.2021.04.032.
[42] Erdohelyi A, Cserenyi J, Solymosi F. Activation of CH_4 and its reaction with CO_2 over supported Rh catalysts. J Catal 1993;141:287–99. https://doi.org/10.1006/jcat.1993.1136.
[43] Ferrandon M, Krause T. Role of the oxide support on the performance of Rh catalysts for the autothermal reforming of gasoline and gasoline surrogates to hydrogen. Appl Catal, A 2006;311:135–45. https://doi.org/10.1016/j.apcata.2006.06.014.
[44] Granlund MZ, Jansson K, Nilsson M, Dawody J, Pettersson LJ. Evaluation of Co, La, and Mn promoted Rh catalysts for autothermal reforming of commercial diesel. Appl Catal, B 2014;154–155:386–94. https://doi.org/10.1016/j.apcatb.2014.02.043.
[45] Hbaieb K. Exploring strontium titanate as a reforming catalyst for dodecane. Appl Nanosci 2016;6:847–54. https://doi.org/10.1007/s13204-015-0494-7.
[46] Hbaieb K, Rashid KKA, Kooli F. Hydrogen production by autothermal reforming of dodecane over strontium titanate based perovskite catalysts. Int J Hydrogen Energy 2017;42:5114–24. https://doi.org/10.1016/j.ijhydene.2016.11.127.
[47] Jeon Y, Lee C, Rhee J, Lee G, Myung JH, Park M, et al. Autothermal reforming of heavy-hydrocarbon fuels by morphology controlled perovskite catalysts using carbon templates. Fuel 2017;187:446–56. https://doi.org/10.1016/j.fuel.2016.09.065.
[48] Lee S, Bae M, Bae J, Katikaneni SP. Ni-Me/Ce0.9Gd0.1O2-x (Me: Rh, Pt and Ru) catalysts for diesel pre-reforming. Int J Hydrogen Energy 2015;40:3207–16. https://doi.org/10.1016/j.ijhydene.2014.12.113.
[49] Lee WS, Ju DG, Jung SY, Lee SC, Ha DS, Hwang BW, et al. N-dodecane autothermal reforming properties of Ni-Al based catalysts prepared by various methods. Top Catal 2017;60:727–34. https://doi.org/10.1007/s11244-017-0777-1.
[50] Liu L, Hong L. Nickel phosphide catalyst for autothermal reforming of surrogate gasoline fuel. AIChE J 2011;57:3143–52. https://doi.org/10.1002/aic.12505.
[51] Liu L, Hong L. Ni/Ce1−xMx catalyst generated from metallo-organic network for autothermal reforming of diesel surrogate. Appl Catal, A 2013;459:89–96. https://doi.org/10.1016/j.apcata.2013.04.012.
[52] Mark MF, Maier WF. CO_2-reforming of methane on supported Rh and Ir catalysts. J Catal 1996;164:122–30. https://doi.org/10.1006/jcat.1996.0368.
[53] Shoynkhorova TB, Rogozhnikov VN, Ruban NV, Shilov VA, Potemkin DI, Simonov PA, et al. Composite Rh/$Zr_{0.25}Ce_{0.75}O_2$-Δ-η-Al_2O_3/Fecralloy wire mesh honeycomb module for natural gas, LPG and diesel catalytic conversion to syngas. Int J Hydrogen Energy 2019;44:9941–8. https://doi.org/10.1016/j.ijhydene.2018.12.148.
[54] Shoynkhorova TB, Rogozhnikov VN, Simonov PA, Snytnikov PV, Salanov AN, Kulikov AV, et al. Highly dispersed Rh/$Ce_{0.75}Zr_{0.25}O_2$-δ-η-Al_2O_3/FeCrAl wire mesh catalyst for autothermal n-hexadecane reforming. Mater Lett 2018;214:290–2. https://doi.org/10.1016/j.matlet.2017.12.017.
[55] Shoynkhorova TB, Simonov PA, Potemkin DI, Snytnikov PV, Belyaev VD, Ishchenko AV, et al. Highly dispersed Rh-, Pt-, Ru/$Ce_{0.75}Zr_{0.25}O_2$−Δ catalysts prepared by sorption-hydrolytic deposition for diesel fuel reforming to syngas. Appl Catal, B 2018;237:237–44. https://doi.org/10.1016/j.apcatb.2018.06.003.
[56] Shoynkhorova TB, Snytnikov PV, Simonov PA, Potemkin DI, Rogozhnikov VN, Gerasimov EY, et al. From alumina modified Rh/$Ce_{0.75}Zr_{0.25}O_2$-Δ catalyst towards composite Rh/$Ce_{0.75}Zr_{0.25}O_2$-Δ-η-Al_2O_3/FeCrAl catalytic system for diesel conversion to syngas. Appl Catal, B 2019:40–8. https://doi.org/10.1016/j.apcatb.2018.12.037.
[57] Wei J, Iglesia E. Structural requirements and reaction pathways in methane activation and chemical conversion catalyzed by rhodium. J Catal 2004;225:116–27. https://doi.org/10.1016/j.jcat.2003.09.030.
[58] Xie JY, Sun XJ, Barrett L, Walker BR, Karote DR, Langemeier JM, et al. Autothermal reforming and partial oxidation of n-hexadecane via Pt/Ni bimetallic catalysts on ceria-based supports. Int J Hydrogen Energy 2015;40:8510–21. https://doi.org/10.1016/j.ijhydene.2015.04.139.
[59] Shilov VA, Rogozhnikov VN, Ruban NV, Potemkin DI, Simonov PA, Shashkov MV, et al. Biodiesel and hydrodeoxygenated biodiesel autothermal reforming over Rh-containing structured catalyst. Catal Today 2020. https://doi.org/10.1016/j.cattod.2020.06.080.
[60] Shilov VA, Rogozhnikov VN, Zazhigalov SV, Potemkin DI, Belyaev VD, Shashkov MV, et al. Operation of Rh/Ce0.75Zr0.25O2-δ-η-Al2O3/FeCrAl wire mesh honeycomb catalytic modules in diesel steam and autothermal reforming. Int J Hydrogen Energy 2021. https://doi.org/10.1016/j.ijhydene.2021.02.092.
[61] Potemkin DI, Rogozhnikov VN, Ruban NV, Shilov VA, Simonov PA, Shashkov MV, et al. Comparative study of gasoline, diesel and biodiesel autothermal reforming over Rh-based FeCrAl-supported composite catalyst. Int J Hydrogen Energy 2020;45:26197–205. https://doi.org/10.1016/j.ijhydene.2020.01.076.
[62] Rogozhnikov VN, Potemkin DI, Ruban NV, Shilov VA, Salanov AN, Kulikov AV, et al. Post-mortem characterization of Rh/Ce0.75Zr0.25O2/Al2O3/FeCrAl wire mesh composite catalyst for diesel autothermal reforming. Mater Lett 2019;257. https://doi.org/10.1016/j.matlet.2019.126715.
[63] Ruban NV, Potemkin DI, Rogozhnikov VN, Shefer KI, Snytnikov PV, Sobyanin VA. Rh- and Rh–Ni–MgO-based structured catalysts for on-board syngas production via gasoline processing. Int J Hydrogen Energy 2021. https://doi.org/10.1016/j.ijhydene.2021.01.183.
[64] Zazhigalov SV, Shilov VA, Rogozhnikov VN, Potemkin DI, Sobyanin VA, Zagoruiko AN, et al. Modeling of hydrogen production by diesel reforming over Rh/Ce0.75Zr0.25O2-δ-η-Al2O3/FeCrAl wire mesh honeycomb catalytic module. Catal Today 2020. https://doi.org/10.1016/j.cattod.2020.11.015.
[65] Han G, Bae M, Cho S, Bae J. Start-up strategy of a diesel reformer using the decomposition heat of hydrogen peroxide for subsea applications. J Power Sources 2020:448. https://doi.org/10.1016/j.jpowsour.2019.227465.
[66] Han G, Lee K, Ha S, Bae J. Development of a thermally self-sustaining kWe-class diesel reformer using hydrogen peroxide for hydrogen production in low-oxygen environments. J Power Sources 2016;326:341–8. https://doi.org/10.1016/j.jpowsour.2016.07.013.
[67] Han G, Lee S, Bae J. Diesel autothermal reforming with hydrogen peroxide for low-oxygen environments. Appl Energy 2015;156:99–106. https://doi.org/10.1016/j.apenergy.2015.06.036.
[68] Peters R. Identification and thermodynamic analysis of reaction pathways of methylal and OME-n formation. Energy 2017;138:1221–46. https://doi.org/10.1016/j.energy.2017.07.050.
[69] Burger K. A novel process for the production of diesel fuel additives by hierarchical design Scientific report series/Laboratory of Engineering Thermodynamics. Technische Universität Kaiserslautern; 2012.
[70] Schmitz N, Ströfer E, Burger J, Hasse H. Conceptual design of a novel process for the production of poly(oxymethylene) dimethyl ethers from formaldehyde and methanol. Ind Eng

Chem Res 2017;56:11519–30. https://doi.org/10.1021/acs.iecr.7b02314.
[71] Deutsch D, Oestreich D, Lautenschütz L, Haltenort P, Arnold U, Sauer J. High purity oligomeric oxymethylene ethers as diesel fuels. Chem Ing Tech 2017;89:486–9. https://doi.org/10.1002/cite.201600158.
[72] Oestreich D, Lautenschütz L, Arnold U, Sauer J. Reaction kinetics and equilibrium parameters for the production of oxymethylene dimethyl ethers (OME) from methanol and formaldehyde. Chem Eng Sci 2017;163:92–104. https://doi.org/10.1016/j.ces.2016.12.037.
[73] Arnold U, Lautenschütz L, Oestreich D, Sauer J. In: Patents G, editor. Verfahren zur Herstellung von Oxymethylendialkylethern und deren Verwendung; 2016.
[74] Schelling H, Ströfer E, Pinkos R, Haunert A, Tebben GD, Hasse H, et al. In: Patens G, editor. Method for producing polyoxymethylene dimethyl ethers; 2007.
[75] Ströfer E, Schelling H, Hasse H, Blagov S. In: Patents G, editor. Verfahren zur Herstellung von Polyoxymethylendialkylethern aus Trioxan und Dialkylether; 2016.
[76] Burger J, Ströfer E, Hasse H. Chemical equilibrium and reaction kinetics of the heterogeneously catalyzed formation of poly(oxymethylene) dimethyl ethers from methylal and trioxane. Ind Eng Chem Res 2012;51:12751–61. https://doi.org/10.1021/ie301490q.
[77] Baranowski CJ, Bahmanpour AM, Héroguel F, Luterbacher JS, Kröcher O. Prominent role of mesopore surface area and external acid sites for the synthesis of polyoxymethylene dimethyl ethers (OME) on a hierarchical H-ZSM-5 zeolite. Catal Sci Technol 2019;9:366–76. https://doi.org/10.1039/C8CY02194E.
[78] Xue Z, Shang H, Zhang Z, Xiong C, Lu C, An G. Efficient synthesis of polyoxymethylene dimethyl ethers on Al-SBA-15 catalysts with different Si/Al ratios and pore sizes. Energy Fuels 2017;31:279–86. https://doi.org/10.1021/acs.energyfuels.6b02255.
[79] Grützner T, Hasse H, Lang N, Siegert M, Ströfer E. Development of a new industrial process for trioxane production. Chem Eng Sci 2007;62:5613–20. https://doi.org/10.1016/j.ces.2007.01.047.
[80] Drunsel J-O, Renner M, Hasse H. Experimental study and model of reaction kinetics of heterogeneously catalyzed methylal synthesis. Chem Eng Res Des 2012;90:696–703. https://doi.org/10.1016/j.cherd.2011.09.014.
[81] Zhang X, Zhang S, Jian C. Synthesis of methylal by catalytic distillation. Chem Eng Res Des 2011;89:573–80. https://doi.org/10.1016/j.cherd.2010.09.002.
[82] Pasel J, Samsun RC, Meißner J, Tschauder A, Peters R. Recent advances in diesel autothermal reformer design. Int J Hydrogen Energy 2020;45:2279–88. https://doi.org/10.1016/j.ijhydene.2019.11.137.
[83] Pasel J, Wohlrab S, Kreft S, Rotov M, Löhken K, Peters R, et al. Routes for deactivation of different autothermal reforming catalysts. J Power Sources 2016;325:51–63. https://doi.org/10.1016/j.jpowsour.2016.06.005.
[84] Pasel J, Samsun RC, Peters R, Thiele B, Stolten D. Long-term stability at fuel processing of diesel and kerosene. Int J Hydrogen Energy 2014;39:18027–36. https://doi.org/10.1016/j.ijhydene.2014.03.148.
[85] Meißner J, Pasel J, Peters R, Samsun RC, Thimm F, Stolten D. Quantitative analysis of sub-ppm traces of hydrocarbons in the product gas from diesel reforming. Int J Hydrogen Energy 2019;44:4020–30. https://doi.org/10.1016/j.ijhydene.2018.12.175.
[86] Pasel J, Samsun RC, Peters R, Stolten D. Fuel processing of diesel and kerosene for auxiliary power unit applications. Energy Fuels 2013;27:4386–94. https://doi.org/10.1021/ef301976f.